Scattering solution of an interacting Hamiltonian for the electronic control of molecular spin qubits

Christian Bunker,[1] Silas Hoffman,[1,*] Jie-Xiang Yu,[2] Xiao-Guang Zhang,[1] and Hai-Ping Cheng[1,†]
[1]*Department of Physics, Center for Molecular Magnetic Quantum Materials, and Quantum Theory Project, University of Florida, Gainesville, Florida 32611, USA*
[2]*School of Physical Science and Technology, Soochow University, Suzhou 215006, China*

(Received 7 November 2022; accepted 16 March 2023; published 17 April 2023)

We theoretically study how a scattered electron can entangle molecular spin qubits (MSQs). This requires solving the inelastic transport of a single electron through a scattering region described by a tight-binding interacting Hamiltonian. We accomplish this using a Green's-function solution. We can model realistic physical implementations of MSQs by parametrizing the tight-binding Hamiltonian with first-principles descriptions of magnetic anisotropy and exchange interactions. We find that, for two-MSQ systems with inversion symmetry, projective measurement of the spin degree of freedom of the scattered electron offers probabilistic control of the degree of entanglement between the MSQs.

DOI: 10.1103/PhysRevA.107.042423

I. INTRODUCTION

Any platform for quantum information processing (QIP) must support entanglement between qubits to achieve quantum speedup [1–3]. Molecular spin qubits (MSQs) formed from a two-level subspace of the electron spin degrees of freedom of a molecular system [4] are a promising platform for QIP because they can be chemically tailored to achieve desired behavior [5,6] and appear well suited for deploying at scale [7]. Although MSQs can be entangled via a Heisenberg-like exchange interaction [8,9], controlling the degree of entanglement experimentally by switching the interaction on and off presents a distinct challenge [7]. It would therefore be beneficial to engineer an alternative method to control of the degree of entanglement between MSQs.

A promising method from the solid-state qubit community is to use an ancillary electron to mediate the entanglement. In one proposal, a localized ancillary electron has an exchange interaction with two qubits for a certain time interval before being removed [10–12]. Control of the time interval then allows the experimenter to control the degree of entanglement between the qubits [10–12] without needing to switch the Heisenberg-like exchange on and off. However, managing the precise time intervals involved remains experimentally challenging [10].

Alternatively, a delocalized ancillary electron (DAE), sourced by a metallic reservoir, can scatter from two qubits to entangle them [10]. This allows the degrees of freedom of the DAE itself to control the degree of entanglement between the qubits, e.g., via projective measurement [13–15], replacing the need for precise time intervals [10,16]. In order to differentiate the proposal of using a *localized* ancillary electron versus a *delocalized* ancillary electron to mediate entanglement, we refer to the latter as the "scattering proposal." In the scattering proposal, schemes for generating Bell states [14,15] and implementing two-qubit gates [17,18] have been theoretically demonstrated. However, because the magnetic anisotropy and Heisenberg-like exchange interactions present in MSQs enable inelastic scattering, addressing MSQs within the scattering proposal presents a distinct theoretical challenge. It therefore remains unclear whether a DAE could entangle MSQs.

Upon developing theoretical tools to overcome this challenge, in this paper we demonstrate that a DAE can mediate entanglement within the scalable, tunable platform offered by MSQs. In Sec. II, we outline our Green's-function solution for scattering from a tight-binding interacting Hamiltonian. In Sec. III we demonstrate a scheme by which a projective measurement of the DAE controls the degree of entanglement between two MSQs. We enumerate the conditions necessary for this scheme and show that the incoming kinetic energy of the DAE provides a convenient degree of freedom for optimizing its probability of success. Applying our scheme to a realistic physical implementation of two MSQs, we explore the molecular characteristics best suited for controlling the degree of entanglement before discussing several real molecular systems which could be used to realize this proposal.

II. METHOD

We now formulate a Green's-function solution to the problem of a DAE scattering from two spin-s particles with which it can interact. It is prevalent in the literature [14–18] to solve these types of problems with a wave-function matching approach in continuous space following Ref. [19]. This is only feasible with analytically solvable scattering potentials. In contrast, the tight-binding approach of Ref. [20] can be connected to first-principles calculations done with atomic orbital basis sets and can be implemented numerically in order to handle arbitrarily complicated systems. We adopt this

*silas.hoffman@ufl.edu
†hping@ufl.edu

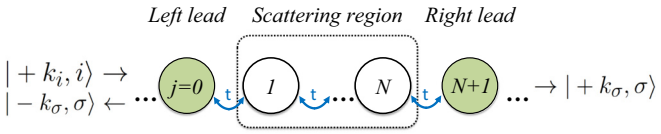

FIG. 1. Setup of the one-dimensional scattering problem as an infinite tight-binding chain with nearest-neighbor hopping.

approach in order to consider realistic physical implementations of MSQs.

Our scattering setup, sketched in Fig. 1, consists of a single DAE in a one-dimensional wire discretized into sites $j \in \mathbb{Z}$ separated by lattice spacing a. These sites form a complete spatial basis $|j\rangle$. The wire could be realized by a single wall carbon nanotube (SWCNT) [21] or a silicon nanowire [22] exhibiting ballistic transport. The left (right) lead is a noninteracting region of the wire consisting of identical sites $j \leqslant 0$ ($j > N$) where the DAE wave function is a plane wave. The scattering region consists of sites $j = 1, \ldots, N$ where the DAE wave function is no longer a plane wave due to interactions with other particles and external potentials. Although the wire is infinite for our purposes, in practice it would eventually contact a metallic system on either side, as in SWCNT spin valve devices [23,24].

Our setup is described by the infinite-dimensional tight-binding Hamiltonian

$$\hat{H} = \sum_{j=-\infty}^{\infty} (\boldsymbol{\varepsilon}_j |j\rangle\langle j| - \mathbf{t}|j\rangle\langle j-1| - \mathbf{t}|j-1\rangle\langle j|). \quad (1)$$

Here boldfaced operators such as $\boldsymbol{\varepsilon}_j$ act on three-particle spin states $|\sigma\rangle$, while operators with hats act on both $|\sigma\rangle$ and spatial states $|j\rangle$. Specifically, each $\boldsymbol{\varepsilon}_j$ is an operator in spin space describing the spin physics and on-site energy of site j. Because the sites in the leads are all identical, $\boldsymbol{\varepsilon}_j = \boldsymbol{\varepsilon}_0$ for $j \leqslant 0$ or $j > N$.

We will now put Eq. (1) in a finite-dimensional form by taking advantage of the periodicity of the leads. Consider the semi-infinite, periodic Hamiltonian

$$\hat{H}^{(M)} = \sum_{j=-\infty}^{M} (\boldsymbol{\varepsilon}_0 |j\rangle\langle j| - \mathbf{t}|j\rangle\langle j-1| - \mathbf{t}|j-1\rangle\langle j|). \quad (2)$$

Clearly $\hat{H}^{(0)}$ describes the left lead. We can associate with $\hat{H}^{(M)}$ a Green's function $\hat{g}^{(M)} = (E\hat{I} - \hat{H}^{(M)})^{-1}$ and a surface Green's function [25,26]

$$\mathbf{g}^{(M)}_{M,M} = \langle M|(E\hat{I} - \hat{H}^{(M)})^{-1}|M\rangle. \quad (3)$$

Because $\hat{H}^{(M+1)}$ can be constructed by adding a single site to $\hat{H}^{(M)}$, its Green's function $\hat{g}^{(M+1)}$ satisfies

$$\begin{pmatrix} E\hat{I} - \hat{H}^{(M)} & \hat{t}^\dagger \\ \hat{t} & E\mathbf{I} - \boldsymbol{\varepsilon}_0 \end{pmatrix} \hat{g}^{(M+1)} = \begin{pmatrix} \hat{I} & 0 \\ 0 & \mathbf{I} \end{pmatrix} \quad (4)$$

where $\hat{t} = \mathbf{t}|M+1\rangle\langle M|$. Solving Eq. (4), we obtain [20]

$$\left(E\mathbf{I} - \boldsymbol{\varepsilon}_0 - \mathbf{t}\mathbf{g}^{(M)}_{M,M}\mathbf{t}\right)\mathbf{g}^{(M+1)}_{M+1,M+1} = \mathbf{I}. \quad (5)$$

At the same time, the periodicity of $\hat{H}^{(M)}$ means that $\hat{H}^{(M)} = \hat{H}^{(M+1)}$. As a result, $\mathbf{g}^{(M)}_{M,M}$ and $\mathbf{g}^{(M+1)}_{M+1,M+1}$ represent the same quantity, the surface Green's function of a semi-infinite lead. In particular, the surface Green's function of the left lead $\mathbf{g}^{(0)}_{00} \equiv \mathbf{g}_L$ obeys the self-consistency condition [20]

$$(E\mathbf{I} - \boldsymbol{\varepsilon}_0 - \mathbf{t}\mathbf{g}_L\mathbf{t})\mathbf{g}_L = \mathbf{I}, \quad (6)$$

which in general can be solved iteratively [27,28].

We now choose as our basis the eigenstates of the system when the DAE is not interacting with any particles in the scattering region. In this basis, $\boldsymbol{\varepsilon}_0$ is diagonal. Ignoring spin-orbit effects, the nearest-neighbor hopping will be spin independent, so $\mathbf{t} = t\mathbf{I}$. As a result, we can solve for the diagonal elements of Eq. (6) [20]:

$$g_{L\sigma\sigma} = \frac{1}{-t}\left[\frac{E - \varepsilon_{0\sigma\sigma}}{-2t} \pm \sqrt{\left(\frac{E - \varepsilon_{0\sigma\sigma}}{-2t}\right)^2 - 1}\right]. \quad (7)$$

The sign of the square root is chosen so that the sign of $\mathrm{Im}(g_{L\sigma\sigma})$ is negative, corresponding to the retarded surface Green's function.

We now introduce the lead self-energies $\boldsymbol{\Sigma}_L = \mathbf{t}\mathbf{g}_L\mathbf{t} = \boldsymbol{\Sigma}_R$ which are equal due to the inversion symmetry of the leads. Substituting Eq. (7), we obtain

$$\Sigma_{L\sigma\sigma} = -t\left[\frac{E - \varepsilon_{0\sigma\sigma}}{-2t} \pm \sqrt{\left(\frac{E - \varepsilon_{0\sigma\sigma}}{-2t}\right)^2 - 1}\right]. \quad (8)$$

The left lead self-energy, being retarded, encodes an outgoing state, the reflected state. Likewise, the retarded right lead self-energy encodes the transmitted state.

Using the definition of the self-energy, Eq. (6) becomes

$$\mathbf{g}_L = [E\mathbf{I} - (\boldsymbol{\varepsilon}_0 + \boldsymbol{\Sigma}_L)]^{-1}, \quad (9)$$

which shows that from the point of view of the Green's function, the physics of the entire left lead can be compactly represented by an energy dependent potential $\boldsymbol{\Sigma}_L$ at its the surface. An analogous expression holds for the right lead. Thus without loss of generality, the entire system can be described by an effective Hamiltonian [20]

$$\hat{H}' = \sum_{j=1}^{N+1}(\boldsymbol{\varepsilon}_j|j\rangle\langle j| - \mathbf{t}|j\rangle\langle j-1| - \mathbf{t}|j-1\rangle\langle j|) + (\boldsymbol{\varepsilon}_0 + \boldsymbol{\Sigma}_L)|0\rangle\langle 0| + \boldsymbol{\Sigma}_R|N+1\rangle\langle N+1|, \quad (10)$$

so we have succeeded in making Eq. (1) finite dimensional. The corresponding retarded Green's function has elements [20]

$$\hat{G}_{jj'\sigma\sigma'} = (E\hat{I} - \hat{H}')^{-1}_{jj'\sigma\sigma'}. \quad (11)$$

Equation (11) formally solves the scattering problem because the scattering region wave-function coefficients

$$|\psi\rangle = \sum_{j=0}^{N+1} \boldsymbol{\psi}_j|j\rangle = \sum_{j=0}^{N+1}\sum_{\sigma} \psi_{j\sigma}|j\rangle|\sigma\rangle \quad (12)$$

can be generated by a convolution [20]

$$\psi_{j\sigma} = \sum_{j'=0}^{N+1}\sum_{\sigma'} G_{jj'\sigma\sigma'}Q_{j'\sigma'}. \quad (13)$$

In Eq. (13), the retarded Green's function encodes the reflected and transmitted states via the retarded self-energies.

The source vector $\mathbf{Q}_j = \sum_\sigma Q_{j\sigma}|\sigma\rangle$ encodes the incoming state, which we now discuss in more detail.

The incoming state is defined by both the three-particle spin state $|\sigma\rangle = |i\rangle$ and the spatial wave function of the DAE as it impinges on site $j = 0$. The spatial wave function is a plane wave with wave number $+k_i$ where $+$ $(-)$ indicates a right (left) moving state. We therefore denote the incoming state as $|+k_i, i\rangle$.

The total energy of the system, E, is always conserved. In general, $E = \varepsilon_{0\sigma\sigma} + K_\sigma$ where $\varepsilon_{0\sigma\sigma}$ is the potential energy of the three-particle spin state $|\sigma\rangle$ and K_σ is the kinetic energy of the DAE plane wave with wave number k_σ, given by the tight-binding dispersion relation

$$K_\sigma = 2t - 2t\cos(k_\sigma a). \tag{14}$$

In practice, the experimenter chooses the incoming kinetic energy K_i by setting the chemical potential of the metallic reservoir that sources the DAE. Without loss of generality, we can set $\varepsilon_{0ii} = 0$, so $K_i = E = \varepsilon_{0\sigma\sigma} + 2t - 2t\cos(k_\sigma a)$. This equality determines the wave number and velocity of all incoming and outgoing spin states:

$$k_\sigma = \frac{1}{a}\cos^{-1}\left(\frac{K_i - \varepsilon_{0\sigma\sigma} - 2t}{-2t}\right), \tag{15}$$

$$v_\sigma = \frac{1}{\hbar}\frac{d}{dk_\sigma}K_\sigma = \frac{2ta}{\hbar}\sin(k_\sigma a). \tag{16}$$

Note that inelastic scattering occurs when the interactions in the scattering region connect states with different wave numbers. These wave numbers and velocities are well defined in the leads because we work in a basis that diagonalizes $\boldsymbol{\varepsilon}_0$; this is the physical reason for choosing such a basis. However, they are not well defined in the scattering region.

Using Eq. (13), we can match the scattering region wave function to the plane waves in the lead. The incoming state is a plane wave:

$$|+k_i, i\rangle = \sum_{j=-\infty}^{0}\sum_\sigma A_\sigma e^{ik_\sigma ja}|j\rangle|\sigma\rangle\,. \tag{17}$$

Here $A_\sigma = A\delta_{\sigma i}$, so A specifies the incoming particle amplitude and $\delta_{\sigma i}$ specifies the incoming spin state. We now introduce the source vector, derived in Eq. (A6):

$$Q_{j\sigma} \equiv \frac{i\hbar}{a}A_\sigma v_\sigma \delta_{j0} \tag{18}$$

where δ_{j0} specifies that the incoming particle impinges on the scattering region from site $j = 0$. The outgoing states, also plane waves, are given by

$$|-k_\sigma, \sigma\rangle = \sum_{j=-\infty}^{0}\sum_\sigma B_\sigma e^{-ik_\sigma ja}|j\rangle|\sigma\rangle, \tag{19}$$

$$|+k_\sigma, \sigma\rangle = \sum_{j=N+1}^{\infty}\sum_\sigma C_\sigma e^{ik_\sigma ja}|j\rangle|\sigma\rangle. \tag{20}$$

Here $|\sigma\rangle$ can be any outgoing spin state, and B_σ and C_σ specify the reflected and transmitted particle amplitude, respectively, in that state.

Since the incoming spin state is always fixed via $A_i = \delta_{\sigma i}$, once t and $K_i = E$ are chosen, we can find the wave number, velocity, and source vector of the incoming particle using Eqs. (15), (16), and (18), respectively. Then once the spin operators $\boldsymbol{\varepsilon}_j$ are specified, we can calculate $\hat{G}$ through Eqs. (8), (10), and (11). $\hat{G}$ solves the scattering problem because the wave-function coefficients from Eq. (13) determine the outgoing states given in Eqs. (19) and (20). We regard K_i/t as an independent variable, so it simply remains to specify $\boldsymbol{\varepsilon}_j$ to achieve this solution. In Appendix A, we show how Eq. (13) generates spin-resolved transmission and reflection coefficients T_σ [Eq. (A11)] and R_σ [Eq. (A13)]. In Appendix B we apply this solution to a simple example system and demonstrate some of its unique capabilities.

III. RESULTS

We now apply our solution to a system of a DAE scattering from two spin-s particles. These particles are due to localized electrons in the molecular system forming a composite spin with $2s + 1$ levels. The generators of rotations are S_l^x, S_l^y, and S_l^z where $l = e$ denotes the DAE and $l = 1, 2$ denotes the spin-s particles. We write these compactly as the vector

$$\mathbf{S}_l = S_l^x\hat{x} + S_l^y\hat{y} + S_l^z\hat{z}. \tag{21}$$

We specify the spin state of the lth particle in terms of the eigenstates $|m_l\rangle_l$ of S_l^z, so that three-particle spin states are written $|m_e\rangle_e|m_1\rangle_1|m_2\rangle_2$. We also define the combined spin operator $\mathbf{S}_{12} = \mathbf{S}_1 + \mathbf{S}_2$ and use s_{12} (m_{12}) for the quantum number corresponding to its magnitude ($\hat{z}$ component). Likewise, we define the total spin operator $\mathbf{S}_T = \mathbf{S}_e + \mathbf{S}_1 + \mathbf{S}_2$ and use s_T (m_T) for the quantum number corresponding to its magnitude ($\hat{z}$ component).

Using an external magnetic field, we can initialize the two spin-s particles in the state $|s\rangle_1|s\rangle_2$. We can also source the DAE from the metallic reservoir in a chosen spin state using a ferromagnetic contact [15]. Thus we can always initialize the system in the spin state

$$|i\rangle \equiv \left|-\frac{1}{2}\right\rangle_e |s\rangle_1|s\rangle_2. \tag{22}$$

Note that the DAE is distinguished from the two spin-s particles because it is an electron, while the two spin-s particles are distinguished from each other by their different spatial locations. As a result, product states such as $|i\rangle$ do not have to be antisymmetrized. We consider only Hamiltonians that are symmetric about the $\hat{z}$ axis in spin space, so m_T is conserved. Subsequently, $|i\rangle$, $|\frac{1}{2}\rangle_e|s-1\rangle_1|s\rangle_2$, and $|\frac{1}{2}\rangle_e|s\rangle_1|s-1\rangle_2$ are the only accessible three-particle spin states. Inspecting these states, we see that conservation of m_T restricts the lth spin-s particle to the two-level subspace $\{|s\rangle_l, |s-1\rangle_l\}$. We can therefore encode a MSQ in this subspace following Ref. [15]. From the accessible three-particle spin states, we can form two new states in which these MSQs are in a Bell state:

$$|\pm\rangle \equiv \left|\frac{1}{2}\right\rangle_e \frac{1}{\sqrt{2}}(|s\rangle_1|s-1\rangle_2 \pm |s-1\rangle_1|s\rangle_2). \tag{23}$$

Note that $|i\rangle$, $|+\rangle$, and $|-\rangle$ are all eigenstates of $\mathbf{S}_{12}^2$, with $s_{12} = 2s$, $2s$, and $2s-1$, respectively. Therefore processes which conserve s_{12} allow $|+\rangle$ to be generated from $|i\rangle$.

As sketched in Fig. 2, we have in mind a scattering geometry wherein the DAE can traverse the system without hopping onto the MSQs. Due to the charge of the electrons forming

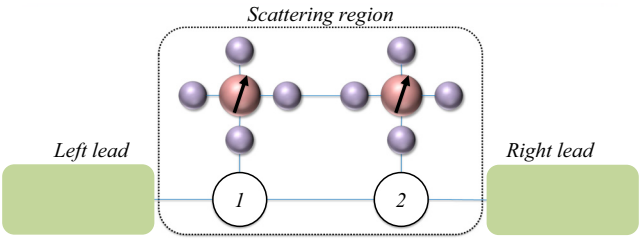

FIG. 2. Physical picture of a conduction electron traversing a scattering region of size $N = 2$ which models a molecular magnetic system. Blue lines represent nonzero hopping matrix elements. The molecular magnetic system hosts two metal atoms (pink spheres) with electronic spin s (black arrows), which are coupled to each other and to the tight-binding sites by ligands (purple spheres).

the MSQs, the Coulombic cost of such hopping will be large. Instead, we treat the hopping onto the MSQs perturbatively using a Schrieffer-Wolff transformation [29] to recover an effectively one-dimensional geometry. Due to this treatment (discussed in more detail in Appendix B and Ref. [30]) the Coulomb interaction between charges occupying the same site becomes an exchange interaction between spins occupying adjacent sites. Therefore in our setup, the first MSQ interacts with site $j = 1$ and the second interacts with site $j = N$. This setup allows us to focus purely on the spin-dependent transport effects rather than electronic transport effects such as the Coulomb blockade (see the supplementary information of Ref. [31]). Physically, this setup could be achieved by laterally coupling a molecular magnetic system to a SWCNT (see Fig. 1 of Ref. [23]).

To implement this model, we specify the $\boldsymbol{\varepsilon}_j$ operators [which determine the Hamiltonian via Eq. (10)] as

$$\boldsymbol{\varepsilon}_j = \frac{J}{\hbar^2}\mathbf{S}_e \cdot (\mathbf{S}_1\delta_{1j} + \mathbf{S}_2\delta_{Nj}). \tag{24}$$

These operators specify a contact interaction in the sense that the DAE only interacts with each MSQ on a single site. The dot product of spin operators has the same form as the Kondo interaction between conduction electrons and a magnetic impurity in a metal [29]. We consider single electron scattering, so there is no Fermi surface and therefore no Kondo physics present in our treatment. However, this Kondo-like form has been applied to single electron scattering [10,14–17,19], so we likewise use this form to maintain continuity with previous works. In the following, we consider the effects of scattering from the Kondo-like interaction of Eq. (24) for systems of two simplified MSQs, then two realistic MSQs with appropriate physical symmetries.

A. Two spin-1/2 MSQs

We first consider the simplest possible implementation of two MSQs: two spin-1/2 particles which do not interact with each other. Each could be realized by a single electron localized to a molecular orbital with strong d or f character. Analogous mesoscopic solid-state systems with magnetic impurities have also been studied in the scattering proposal [10,14–17,19]. The only spin physics present in this system is the Kondo-like interaction between the DAE and the MSQs

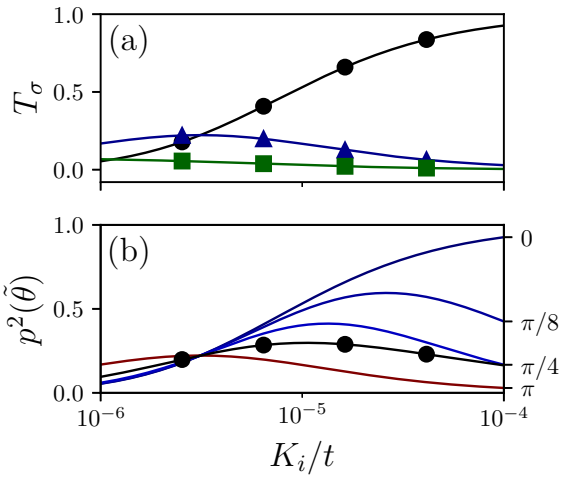

FIG. 3. (a) Transmission coefficients (black circles) T_i, (blue triangles) T_+, and (green squares) $T_- \times 10^5$. The tiny value of T_- shows that the transmission approximately conserves s_{12}. (b) Probability of success [Eq. (37)] at different values of $\tilde{\theta}$, labeled on the right. Black circles show the probability of success averaged over $\tilde{\theta}$, given by Eq. (38). Tight-binding parameters are $N = 2$, $t = 100$ meV, and $J = -0.5$ meV.

[Eq. (24)]. For this interaction, $[\boldsymbol{\varepsilon}_0, \mathbf{S}_{12}^2] = 0$. As a result, we work in the eigenbasis of $\mathbf{S}_{12}^2$, $|\sigma\rangle \in \{|+\rangle, |-\rangle, |i\rangle\}$, and calculate the corresponding transmission coefficients T_+, T_-, and T_i using Eq. (A11). Note that in this basis, $\varepsilon_{0\sigma\sigma}$ is the same for all σ, so the plane-wave wave numbers and velocities given in Eqs. (15) and (16) are spin independent.

In general, each T_σ depends on the DAE's incoming kinetic energy K_i, as well as the quantities J and N appearing in Eq. (24). More precisely, t sets the energy scale, so N, J/t, and K_i/t are the dimensionless parameters which determine T_σ. We first examine the effects of N. Although $N > 1$ is required to keep the two spin-s particles distinguishable, it is useful to first note that if $N = 1$ in Eq. (24), we would have $[\boldsymbol{\varepsilon}_j, \mathbf{S}_{12}^2] = 0$ and so s_{12} would be conserved during the scattering process. As noted earlier, this situation is of interest because $|i\rangle$, in which the MSQs are unentangled, can be scattered into $|+\rangle$, in which the MSQs are in a Bell state. We expect that in the limit of small separation, i.e., $N = 2$, s_{12} will still be approximately conserved. In Fig. 3(a), we show that for a specific $N = 2$ system, T_- never exceeds 10^{-6}. For the remainder of this paper we fix $N = 2$ with the expectation that s_{12} will be approximately conserved. This is confirmed by the small values of T_- in each case.

With $N = 2$ fixed, we examine the effects of J/t. In Ref. [19], the problem of scattering from Eq. (24) is solved in the continuum case for $N = 1$ (i.e., for a single composite spin). This solution, discussed in more detail in Appendix B, approximately maps onto our system in the limit $k_i a \ll 1$ and $N = 2$, in which case we expect $T_+ \approx T_{f,c}$ [Eq. (B3)]. $T_{f,c}$ depends on J/t only through the dimensionless parameter $(J/tk_i a)^2$. Therefore when $T_+ \approx T_{f,c}$, the sign of J/t has no effect, while its magnitude affects the value of $k_i a$ at which T_+ peaks but not the height of the peak. We thus do not investigate different J/t values but focus on $J = -0.5$ meV as measured for molecules laterally coupled to SWCNTs [23].

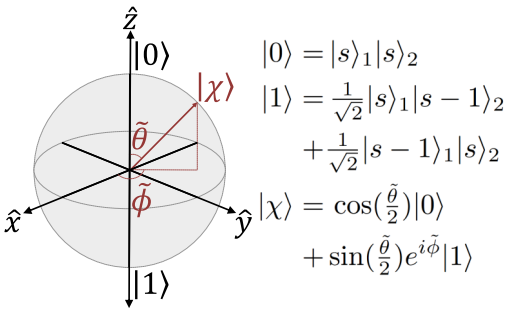

FIG. 4. Depiction of the logical state $|\chi\rangle$ in the Bloch sphere formalism. The north pole is completely unentangled, while the south pole is maximally entangled, so specifying $|\chi\rangle$ controls the degree of entanglement.

Restricting ourselves to $N = 2$ and $J = -0.5$ meV for the rest of this paper, K_i/t is the only free dimensionless parameter affecting T_σ for spin-1/2 MSQs. Furthermore, because s_{12} is conserved only T_i and T_+ are nonzero. The simplest application of this scenario is to generate $|+\rangle$, in which the MSQs are in a Bell state, by projective measurement of the DAE onto spin state $|\frac{1}{2}\rangle_e$ with probability T_+. Similar Bell state generation processes were proposed in Refs. [14,15]. Our results, shown in Fig. 3(a), demonstrate that K_i/t provides a convenient degree of freedom for maximizing the Bell state generation probability T_+ (blue triangles). We observe a peak of $T_+ = 0.22$, consistent with the results of Refs. [14,15].

Beyond Bell state generation, when s_{12} is conserved, the spin degree of the freedom of the DAE controls the degree of entanglement between MSQs. By control of the degree of entanglement we mean that in the logical basis

$$|0\rangle \equiv |s\rangle_1|s\rangle_2, \tag{25}$$

$$|1\rangle \equiv \frac{1}{\sqrt{2}}(|s\rangle_1|s-1\rangle_2 + |s-1\rangle_1|s\rangle_2) \tag{26}$$

we can rotate from $|0\rangle$ to any desired superposition of $|0\rangle$ and $|1\rangle$ (see Ref. [12]). This rotation controls the degree of entanglement because $|0\rangle$ is an unentangled state, easily initialized by application of an external magnetic field along the $\hat{z}$ axis, while $|1\rangle$ is maximally entangled. These form the antipodal points of a Bloch sphere as shown in Fig. 4. As we will show, the DAE's spin degree of freedom exactly specifies the desired superposition and thus controls the degree of entanglement.

Assuming s_{12} is conserved, the transmitted state, given by Eq. (20), is

$$|T\rangle = \sum_{j=N+1}^{\infty} \left(C_i e^{ik_i ja}|j\rangle|i\rangle + C_+ e^{ik_+ ja}|j\rangle|+\rangle\right). \tag{27}$$

Now we perform a projective measurement [13] of the DAE spin along the axis $\hat{n} = (1, \theta, \phi)$ as it is transmitted into the right lead, i.e., at site $j = N + 1$. This has two effects on $|T\rangle$. First, it eliminates the j dependence of the phase between spin states $|i\rangle$ and $|+\rangle$ by projecting the spatial degree of freedom of the DAE onto $|N + 1\rangle$:

$$\begin{aligned}\langle N+1|T\rangle &= e^{ik_i a(N+1)}C_i|i\rangle + e^{ik_+ a(N+1)}C_+|+\rangle \\ &= \sqrt{T_i}\left|-\tfrac{1}{2}\right\rangle_e|0\rangle + \sqrt{T_+}e^{i\phi_+}\left|\tfrac{1}{2}\right\rangle_e|1\rangle.\end{aligned} \tag{28}$$

Here we substituted $|C_\sigma| = \sqrt{T_\sigma}$ and dropped the overall phase $\exp(ik_i a(N + 1) + \arg(C_i))$, but allowed for a complex phase between the two spin states:

$$\exp(i\phi_+) = \exp\left(i(k_+ - k_i)a(N+1) + \arg(C_+) - \arg(C_i)\right). \tag{29}$$

Second, it projects the spin degree of freedom of the DAE onto one of the eigenstates of $\mathbf{S}_e \cdot \hat{n}$, namely [32],

$$|\Uparrow\rangle_e = \cos\left(\frac{\theta}{2}\right)\left|\frac{1}{2}\right\rangle_e + \sin\left(\frac{\theta}{2}\right)e^{i\phi}\left|-\frac{1}{2}\right\rangle_e, \tag{30}$$

$$|\Downarrow\rangle_e = -\sin\left(\frac{\theta}{2}\right)\left|\frac{1}{2}\right\rangle_e + \cos\left(\frac{\theta}{2}\right)e^{i\phi}\left|-\frac{1}{2}\right\rangle_e. \tag{31}$$

Specifically, measuring $\mathbf{S}_e \cdot \hat{n} = -\hbar/2$ yields

$$\begin{aligned}|\chi\rangle &\equiv {}_e\langle\Downarrow|\langle j = N+1|T\rangle \\ &= \cos\left(\frac{\theta}{2}\right)e^{-i\phi}\sqrt{T_i}|0\rangle - \sin\left(\frac{\theta}{2}\right)e^{i\phi_+}\sqrt{T_+}|1\rangle.\end{aligned} \tag{32}$$

Finally, by introducing the logical space angles

$$\tan\left(\frac{\tilde{\theta}}{2}\right) = \sqrt{\frac{T_+}{T_i}}\tan\left(\frac{\theta}{2}\right), \tag{33}$$

$$\tilde{\phi} = \phi + \phi_+ + \pi, \tag{34}$$

we can manipulate Eq. (32) to obtain

$$|\chi\rangle = p(\tilde{\theta})\left[\cos\left(\frac{\tilde{\theta}}{2}\right)|0\rangle + \sin\left(\frac{\tilde{\theta}}{2}\right)e^{i\tilde{\phi}}|1\rangle\right]. \tag{35}$$

The prefactor introduced here is

$$p(\tilde{\theta}) = \sqrt{\frac{T_i T_+}{T_+\cos^2\left(\frac{\tilde{\theta}}{2}\right) + T_i\sin^2\left(\frac{\tilde{\theta}}{2}\right)}}, \tag{36}$$

while the quantity in square brackets is a unit vector on the Bloch sphere [1]. Then for $T_i, T_+ \neq 0$, $\hat{n}$ specifies $|\chi\rangle$ because we can choose any $\tilde{\theta} \in [0, \pi]$ by appropriate choice of θ and any $\tilde{\phi} \in [0, 2\pi]$ by appropriate choice of ϕ. However, to successfully specify $|\chi\rangle$, the projective measurement of the DAE's spatial degree of freedom must return $j = N + 1$, requiring transmission to occur, and the projective measurement of the DAE's spin degree of freedom must return $-\hbar/2$. The combined probability of success for this operation is

$$p^2(\tilde{\theta}) = \frac{T_i T_+}{T_+\cos^2\left(\frac{\tilde{\theta}}{2}\right) + T_i\sin^2\left(\frac{\tilde{\theta}}{2}\right)}. \tag{37}$$

Like all projective measurement methods for generating entanglement, this method produces maximum localizable entanglement [33], but only probabilistically [13].

We plot the probability of success $p^2(\tilde{\theta})$ for representative values of $\tilde{\theta}$ in Fig. 3(b). Note that only $p^2(\tilde{0})$ achieves probability 1, while $p^2(\pi) = T_+$ corresponding to the Bell state generation process discussed previously. The main application of this paper is to control the degree of entanglement by specifying any desired $\tilde{\theta}$, so a useful figure of merit is obtained by averaging $p^2(\tilde{\theta})$ over $\tilde{\theta}$:

$$\overline{p^2} = \frac{1}{\pi}\int_0^\pi \frac{T_i T_+\, d\,\tilde{\theta}}{T_+\cos^2\left(\frac{\tilde{\theta}}{2}\right) + T_i\sin^2\left(\frac{\tilde{\theta}}{2}\right)} = \sqrt{T_i T_+}. \tag{38}$$

In Fig. 3(b), we show how $\overline{p^2}$ varies with K_i/t. This quantity is again convenient for maximizing $\overline{p^2}$. We observe $\max(\overline{p^2}) = 0.30$ which we can analyze in light of our previous assumption that for $k_i a \ll 1$ and $N = 2$, $T_+ \approx T_{f,c}$ [Eq. (B3)] and $T_i \approx T_{nf,c}$ [Eq. (B4)]. Inserting these into Eq. (38), the predicted maximum is $\overline{p^2} = 0.32$, so the observed maximum is reasonable.

B. Two molecular magnetic MSQs

We now consider a more complicated implementation of two MSQs: a molecular magnetic system hosting two metal atoms. Each atom's valence electrons form a composite spin-s particle, where for generality s is left unspecified. As in the previous section, these particles have a Kondo-like interaction with the DAE given by Eq. (24). In addition, these particles have uniaxial magnetic anisotropy and a Heisenberg-like exchange interaction with each other. In specifying the form of these interactions, we recall that only Hamiltonians which are symmetric about the $\hat{z}$ axis in spin space can encode a MSQ in the subspace $\{|s\rangle_l, |s-1\rangle_l\}$. The most general form of $\boldsymbol{\varepsilon}_j$ with this symmetry, to second order in the spin operators, is

$$\boldsymbol{\varepsilon}_j = \frac{1}{\hbar^2}\big[J\mathbf{S}_e \cdot (\mathbf{S}_1\delta_{1j} + \mathbf{S}_2\delta_{Nj}) + D_1\big(S_1^z\big)^2 + D_2\big(S_1^z\big)^2 + J_{12}^x\big(S_1^xS_2^x + S_1^yS_2^y\big) + J_{12}^zS_1^zS_2^z\big]. \tag{39}$$

Equation (39) is block diagonalized by m_T, and we concentrate on the $m_T = 2s - 1/2$ block. In this block, we choose as our basis the eigenbasis of $\mathbf{S}_{12}^2$, namely, $|\sigma\rangle \in \{|+\rangle, |-\rangle, |i\rangle\}$. In this basis,

$$\begin{aligned}\boldsymbol{\varepsilon}_j = {} & \big[2s^2D + (s^2-s)J_{12}^z\big]\mathbf{I} \\ & + \begin{pmatrix} (1-2s)D + sJ_{12}^x & \big(s-\frac{1}{2}\big)\Delta_D & 0 \\ \big(s-\frac{1}{2}\big)\Delta_D & (1-2s)D - sJ_{12}^x & 0 \\ 0 & 0 & sJ_{12}^z \end{pmatrix} \\ & + \frac{J}{2}\begin{pmatrix} s-\frac{1}{2} & \frac{1}{2} & \sqrt{s} \\ \frac{1}{2} & s-\frac{1}{2} & -\sqrt{s} \\ \sqrt{s} & -\sqrt{s} & -s \end{pmatrix}\delta_{j1} \\ & + \frac{J}{2}\begin{pmatrix} s-\frac{1}{2} & -\frac{1}{2} & \sqrt{s} \\ -\frac{1}{2} & s-\frac{1}{2} & \sqrt{s} \\ \sqrt{s} & \sqrt{s} & -s \end{pmatrix}\delta_{jN}, \end{aligned} \tag{40}$$

where $D = (D_1 + D_2)/2$ and $\Delta_D = D_1 - D_2$. The parameters D_1, D_2, J_{12}^x, and J_{12}^z in Eq. (39) can be fit with density functional theory (DFT) to build a model of a molecular system containing spins with a shared axis of uniaxial magnetic anisotropy; see for example Ref. [34].

Since the two particles have the same s, the system has inversion symmetry if $D_1 = D_2$. For the rest of this section, we impose inversion symmetry. This is necessary to diagonalize $\boldsymbol{\varepsilon}_0$ so that s_{12} is a good quantum number. Then because the last line of Eq. (40) approximately conserves s_{12} when $N = 2$, $|i\rangle$ only scatters into itself or $|+\rangle$ as before. However, these two states are no longer degenerate; instead, they are split in energy by

$$\Delta E \equiv \varepsilon_{0++} - \varepsilon_{0ii} = (1-2s)D + s\big(J_{12}^x - J_{12}^z\big). \tag{41}$$

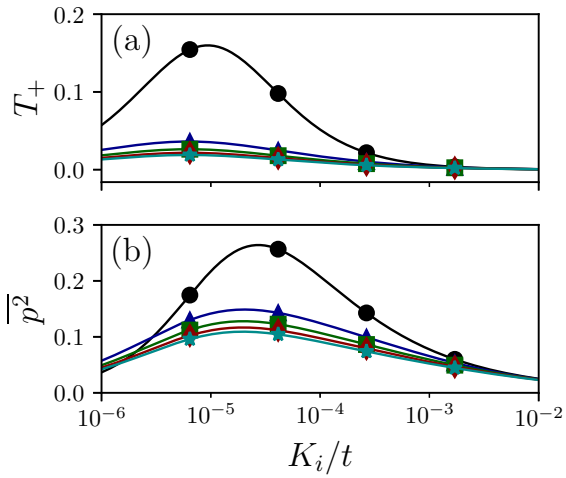

FIG. 5. Dependence of (a) T_+ (T_- is omitted because it never exceeds 10^{-4}) and (b) $\overline{p^2}$ on K_i/t and $\Delta E/t$ when $s = 1$. Tight-binding parameters are $N = 2$, $t = 100\,\text{meV}$, $J = -0.5\,\text{meV}$, and $J_{12}^x = J_{12}^z = 1.0\,\text{meV}$. By choice of D we set (black circles) $\Delta E/t = 0.0$, (blue triangles) $\Delta E/t = -0.001$, (green squares) $\Delta E/t = -0.002$, (red diamonds) $\Delta E/t = -0.003$, and (cyan stars) $\Delta E/t = -0.004$.

Inspecting Eq. (40) when $\Delta_D = 0$, we see that aside from J/t, which we have already discussed, the only dimensionless parameters that affect the transmission coefficients are K_i/t, $\Delta E/t$, and s. Recalling that the figure of merit for our scheme by which the DAE controls the degree of entanglement is $\overline{p^2}$, we now explore how each of these affects $\overline{p^2}$.

In the $s = 1/2$ case (Fig. 3) we saw that $\overline{p^2}$ increases with increasing K_i/t, reaches a maximum, then decreases. This is also the case for the molecular magnetic system when $\Delta E/t \geqslant 0$ as shown in Fig. 5. When $\Delta E/t < 0$, the behavior is very different because transmission into the $|+\rangle$ state is energetically forbidden when $K_i < \Delta E$, as shown in Fig. 6.

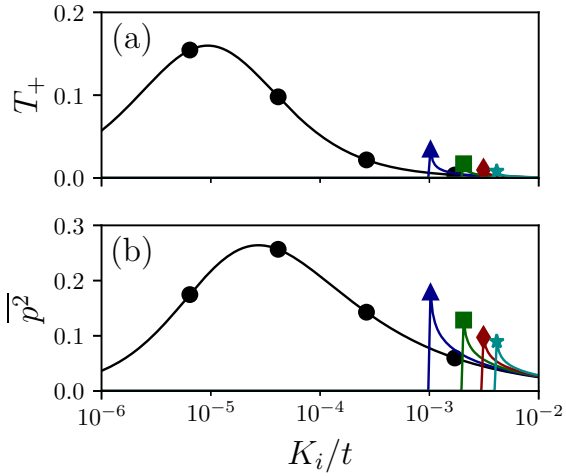

FIG. 6. Dependence of (a) T_+ (T_- is omitted because it never exceeds 10^{-4}) and (b) $\overline{p^2}$ on K_i/t and $\Delta E/t$ when $s = 1$. Tight-binding parameters are $N = 2$, $t = 100\,\text{meV}$, $J = -0.5\,\text{meV}$, and $J_{12}^x = J_{12}^z = 1.0\,\text{meV}$. By choice of D we set (black circles) $\Delta E/t = 0.0$, (blue triangles) $\Delta E/t = 0.001$, (green squares) $\Delta E/t = 0.002$, (red diamonds) $\Delta E/t = 0.003$, and (cyan stars) $\Delta E/t = 0.004$.

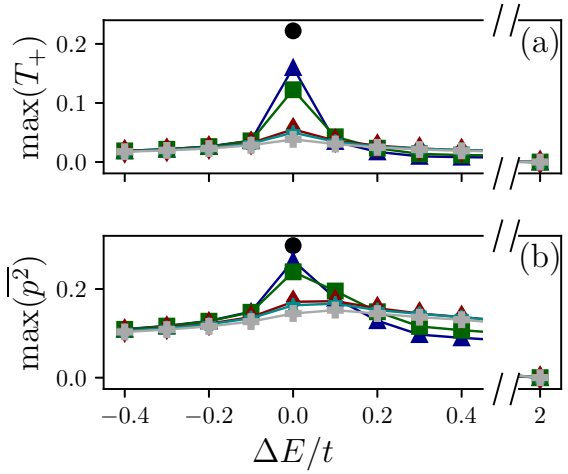

FIG. 7. Maxima of (a) T_+ and (b) $\overline{p^2}$ over 199 values of $\log_{10}(K_i/t)$ evenly spaced on the interval $[-6, -2]$ for spin-s particles at different $\Delta E/t$. Black circles show $s = 1/2$, for which only $\Delta E/t = 0.0$ is possible, with tight-binding parameters $N = 2$, $t = 100\,\text{meV}$, and $J = -0.5\,\text{meV}$. Blue triangles show $s = 1$, (green squares) $s = 3/2$, (red diamonds) $s = 4$, (cyan stars) $s = 9/2$, and (gray pluses) $s = 6$, with tight-binding parameters $N = 2$, $t = 100\,\text{meV}$, $J = -0.5\,\text{meV}$, $J^x_{12} = J^z_{12} = 1.0\,\text{meV}$, and D variable.

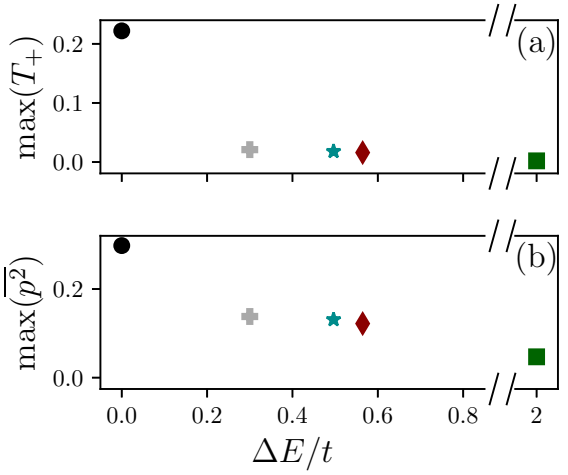

FIG. 8. Maxima of (a) T_+ and (b) $\overline{p^2}$ for real molecular magnetic systems. Tight-binding parameters are $N = 2$, $t = 100\,\text{meV}$, and $J = -0.5\,\text{meV}$ throughout. Green square shows a MnPc with $s = 3/2$, $D = -0.99\,\text{meV}$, and $J^x_{12} = J^z_{12} = -0.77\,\text{meV}$ [35]. Red diamond shows a Mn(III) dimer with $s = 4$, $D = -0.08\,\text{meV}$, and $J^x_{12} = J^z_{12} = -0.53\,\text{meV}$ [36]. Cyan star shows a Mn_4 dimer, with $s = 9/2$, $D = -0.06\,\text{meV}$, and $J^x_{12} = J^z_{12} = 0.009\,\text{meV}$ [37]. Gray plus shows an Mn_3 dimer, with $s = 6$, $D = -0.03\,\text{meV}$, and $J^x_{12} = J^y_{12} = -0.006\,\text{meV}$ [34].

However, regardless of the sign of $\Delta E/t$, $\overline{p^2}$ has a single maximum over the domain of K_i/t which we denote $\max(\overline{p^2})$. We can always tune K_i/t to achieve $\max(\overline{p^2})$. The same is true for T_+, which quantifies the Bell state generation probability.

In Fig. 7, we explore the dependence of $\max(\overline{p^2})$ and $\max(T_+)$ on $\Delta E/t$ and s in order to determine the molecular characteristics most suitable for our scheme by which the DAE controls the degree of entanglement and for generating Bell states. We plot the $s = 1/2$ result $\max(\overline{p^2}) = 0.30$ (black circles) for reference. We then plot data for $s = 1$, 3/2, 4, 9/2, and 6. Note that $\max(T_+)$ and $\max(\overline{p^2})$ tend to decrease with increasing s. This is consistent with previous results, e.g., Fig. 2 of Ref [15]. Also, as s increases towards the classical limit, the dependence of $\max(T_+)$ and $\max(\overline{p^2})$ on s decreases.

IV. DISCUSSION AND CONCLUSION

We showed that molecular magnetic systems hosting two metal atoms with a shared axis of symmetry in spin space are suitable for encoding two MSQs. Using a simple model of two MSQs, we demonstrated that when scattering from the MSQs conserves s_{12}, it is possible to maximally entangle them using a DAE. Moreover, we were able to control the degree of entanglement between the MSQs via a projective measurement of the spin degree of freedom of the DAE. Although the control scheme we presented is probabilistic, the experimenter immediately sees whether it has succeeded, and we can quantify the probability of success with $\overline{p^2}$ [Eq. (38)].

To motivate discussion about the feasibility of implementing our control scheme in real molecular magnetic systems, we next turned to a more realistic model of two MSQs. This model included the uniaxial magnetic anisotropy and Heisenberg-like exchange effects typical of molecular magnetic systems, but control of the degree of entanglement was still possible. We explored the dependence of $\overline{p^2}$ on s, the spin of the MSQs, and ΔE, the energy splitting. Figure 7 shows that, in the $N = 2$, $t = 100\,\text{meV}$, and $J = -0.5\,\text{meV}$ scenario we examined, systems with $s \leqslant 3/2$ and $|\Delta E| \ll 1\,\text{meV}$ are best suited for our control scheme. More generally, systems with $|\Delta E/J| \ll 1$ are desirable. If such systems cannot be found, they could be engineered thanks to the chemical tunability of molecular QIP platforms. DFT has shown that charge doping [38] or the addition of symmetry-breaking ligands [39] can lower the magnitude of the magnetic anisotropy of single molecule magnets (SMMs), which would in turn decrease $|\Delta E|$ according to Eq. (41). Alternatively, one can use external experimental parameters to tune ΔE, e.g., with applied magnetic fields or through the dependence of J^x_{12} on external pressure [34].

With this in mind, we now discuss several candidate molecular magnetic systems for implementing our scheme by which the DAE controls the degree of entanglement. We first recall that the setup we have in mind involves a molecular system laterally coupled to a conducting region which is long and narrow along the $\hat{z}$ axis (e.g., a SWCNT as in Fig. 1 of Ref. [23]) with the MSQs spatially separated along the $\hat{z}$ axis as shown in Fig. 2. A dimer of two identical SMMs held together by a linker naturally fits this setup because it can be placed onto the SWCNT with the intermolecular axis parallel to the $\hat{z}$ axis. Some examples are an $s = 4$ Mn(III) dimer [36], an $s = 9/2$ Mn_4 dimer [37], and an $s = 6$ Mn_3 dimer [34]. All have the requisite symmetries of Eq. (39) with $D_1 = D_2$ and $|\Delta E|$ of order 0.1 meV as desired. However, as shown in Fig. 8 their $\max(\overline{p^2})$ values remain well below the $s = 1/2$ result due to their large s values. Our results suggest that much improved

$\overline{p^2}$ could be achieved by a SMM dimer with $s \leqslant 3/2$; however, no such complexes have come to our attention.

Metal-phthalocyanines (MPc's) in which organic ligands surround a central metal ion [35] are another real molecular system that offers a potential realization of our scheme. MPc's are already of interest for QIP applications [31,40]. Isolated MPc's are typically planar and could be placed side by side atop the SWCNT to achieve our desired setup. Choice of the metal ion allows us to select a lower spin; for example MnPc has $s = 3/2$ [35] while VOPc has $s = 1/2$ [40]. While the former is hampered by an unusually large energy splitting of $\Delta E = -1.98\,\text{meV}$, the latter has no energy splitting by virtue of being $s = 1/2$ and thus appears especially promising for our scheme by which the DAE controls the degree of entanglement.

Although we were able to take advantage of the fact that the Hamiltonian describing the interaction between the DAE and two spin-s particles conserves m_T to encode a MSQ in the two-level subspace of the $(2s+1)$-dimensional eigenspace of S_l^z, there are limitations to this encoding. Specifically, all four two-MSQ basis states should be accessible in order for the MSQs to be fully functional, but conservation of m_T causes $|s-1\rangle_1|s-1\rangle_2$ to be inaccessible. In principle, full functionality can still be achieved if each qubit can be manipulated individually, e.g., with microwaves [41]. However, such manipulation would also have to incorporate conservation laws in some way to stay in the two-level subspace of the larger Hilbert space, which poses an additional challenge.

ACKNOWLEDGMENTS

We are grateful for helpful discussions with Garnet Chan and Eric Switzer. This work was supported as part of the Center for Molecular Magnetic Quantum Materials, an Energy Frontier Research Center funded by the U.S. Department of Energy, Office of Science, Basic Energy Sciences under Grant No. DE-SC0019330. Computations were done using the utilities of the National Energy Research Scientific Computing Center and University of Florida Research Computing.

APPENDIX A: DERIVATIONS

1. Source vector

The role of $\hat{G}$ [Eq. (11)] is to connect the incoming state [Eq. (17)] to the outgoing states [Eqs. (19) and (20)]. Although the incoming and outgoing states are boundary conditions in the mathematical sense, it is important to note that only the incoming state is chosen by the experimenter. The outgoing states are determined by the incoming state and the scattering potential. The source vector [Eq. (18)] encodes the incoming state, while the outgoing states are encoded by $\hat{G}$ itself.

The eigenstates in the left lead are plane waves specified by A_σ and B_σ, the incoming and reflected particle amplitudes in state $|\sigma\rangle$. By working in the basis that diagonalizes $\boldsymbol{\varepsilon}_0$, we ensure these plane waves have well-defined wave numbers and velocities given by Eqs. (15) and (16). As a result, the wave function in the left lead takes the general form

$$|\psi\rangle = \sum_{j=-\infty}^{0} \sum_{\sigma} \left(A_\sigma e^{ik_\sigma ja} + B_\sigma e^{-ik_\sigma ja}\right)|j\rangle|\sigma\rangle. \tag{A1}$$

We could obtain a boundary condition at site $j = 0$ directly from Eq. (A1), but it would not properly distinguish the incoming state from the reflected state. Instead, we can use the Schrödinger equation to define a source vector as follows.

Applying Eq. (1) to Eq. (12) yields the Schrödinger equation at $j = 1$:

$$(E\mathbf{I} - \boldsymbol{\varepsilon}_0)\boldsymbol{\psi}_0 + \mathbf{t}\boldsymbol{\psi}_1 + \mathbf{t}\boldsymbol{\psi}_{-1} = 0 \tag{A2}$$

where E is the total energy of the system. Assuming that the hopping is spin independent, $\mathbf{t}$ is diagonal. Since we already diagonalized $\boldsymbol{\varepsilon}_0$, Eq. (A2) simplifies to

$$(E - \varepsilon_{0\sigma\sigma})\psi_{0\sigma} + t(\psi_{1\sigma} + \psi_{-1\sigma}) = 0. \tag{A3}$$

From Eq. (A1), we have $\psi_{-1\sigma} = A_\sigma e^{-ik_\sigma a} + B_\sigma e^{ik_\sigma a}$ and $\psi_{0\sigma} = A_\sigma + B_\sigma$. With these substitutions, Eq. (A3) can be written as

$$E\psi_{0\sigma} - \left(\varepsilon_{0\sigma\sigma}\psi_{0\sigma} - t\psi_{1\sigma} - te^{ik_\sigma a}\psi_{0\sigma}\right) = A_\sigma t\left(e^{ik_\sigma a} - e^{-ik_\sigma a}\right). \tag{A4}$$

Following Ref. [42], Eq. (A4) can be rewritten by defining on the left-hand side a retarded self-energy

$$\begin{aligned}\Sigma_{L\sigma\sigma} &= -te^{ik_\sigma a} \\ &= -t\left[\frac{E - \varepsilon_{0\sigma\sigma}}{-2t} + \sqrt{\left(\frac{E - \varepsilon_{0\sigma\sigma}}{-2t}\right)^2 - 1}\right],\end{aligned} \tag{A5}$$

and on the right-hand side, using Eq. (16), a source vector

$$\begin{aligned}Q_{0\sigma} &= A_\sigma t\left(e^{ik_\sigma a} - e^{-ik_\sigma a}\right) \\ &= 2iA_\sigma t\sin(k_\sigma a) = \frac{i\hbar}{a}A_\sigma v_\sigma.\end{aligned} \tag{A6}$$

Equations (A5) and (A6) recover Eqs. (8) and (18), respectively. Substituting them yields the Schrödinger equation with an effective Hamiltonian and a source term,

$$E\psi_{0\sigma} - [(\varepsilon_{0\sigma\sigma} - \Sigma_{L\sigma\sigma})\psi_{0\sigma} - t\psi_{1\sigma}] = Q_{0\sigma}, \tag{A7}$$

so that as usual the Green's function, which solves the Schrödinger equation with an identity source, can be convoluted with the source term to solve Eq. (A7).

2. Transmission and reflection coefficients

Enforcing continuity of Eq. (12) with Eqs. (17) and (19) at $j = 0$ and with Eq. (20) at $j = N + 1$ leads to the boundary conditions

$$\psi_{0,\sigma} = A_\sigma + B_\sigma, \tag{A8}$$

$$\psi_{N+1,\sigma} = C_\sigma e^{ik_\sigma(N+1)a}. \tag{A9}$$

We can match the coefficients of each spin state individually because $j = 0$ and $N + 1$ are in the leads, where there are no interactions to couple different spin states.

The transmission (reflection) coefficients can now be calculated from the ratio of transmitted (reflected) flux to

incoming flux. The incoming flux is $\sum_{\sigma'} A_{\sigma'} A_{\sigma'} v_{\sigma'}$ while the transmitted flux in spin state $|\sigma\rangle$ is $|C_\sigma|^2 v_\sigma$. Inserting Eqs. (13), (18), and (A9), we have

$$T_\sigma = \frac{|C_\sigma|^2 v_\sigma}{\sum_{\sigma'} A_{\sigma'} A_{\sigma'} v_{\sigma'}}$$
$$= \frac{\left|\frac{i\hbar}{a}\sum_{\sigma''} G_{N+1,0,\sigma,\sigma''} A_{\sigma''} v_{\sigma''}\right|^2 v_\sigma}{\sum_{\sigma'} A_{\sigma'} A_{\sigma'} v_{\sigma'}} \quad \text{(A10)}$$
$$= \frac{\hbar^2}{a^2} |G_{N+1,0,\sigma,i}|^2 v_\sigma v_i. \quad \text{(A11)}$$

Note that Eq. (A10) is general while Eq. (A11) is for the case of a single incoming spin state, $A_\sigma = A\delta_{\sigma i}$. Similarly, the reflected flux in spin state $|\sigma\rangle$ is $|B_\sigma|^2 v_\sigma$, so using Eqs. (13), (18), and (A8), we have

$$R_\sigma = \frac{|B_\sigma|^2 v_\sigma}{\sum_{\sigma'} A_{\sigma'} A_{\sigma'} v_{\sigma'}}$$
$$= \frac{\left|\frac{i\hbar}{a}\sum_{\sigma'} G_{0,0,\sigma,\sigma''} A_{\sigma''} v_{\sigma''} - A_\sigma\right|^2 v_\sigma}{\sum_{\sigma'} A_{\sigma'} A_{\sigma'} v_{\sigma'}} \quad \text{(A12)}$$
$$= \left|\frac{i\hbar}{a} G_{0,0,\sigma,i} v_i - \delta_{\sigma i}\right|^2 \frac{v_\sigma}{v_i}. \quad \text{(A13)}$$

Again, Eq. (A13) is for a single incoming spin state.

APPENDIX B: SPIN-DEPENDENT SCATTERING

As a simple example of a spin-dependent scattering problem, consider the DAE impinging on a scattering region containing a single spin-s particle. When the DAE is in the scattering region, its spin can interact with the spin of the spin-s particle. Reference [19] treats this problem for the case $s = 1/2$ using the continuum Hamiltonian $H_c = K_{i,c} + \varepsilon_c$. Here the subscript c specifies the continuum case, $K_{i,c}$ is the incoming kinetic energy of the DAE, and the continuum scattering potential is

$$\varepsilon_c = \frac{J a_c}{\hbar^2} \mathbf{S}_e \cdot \mathbf{S}_1 \delta(x). \quad \text{(B1)}$$

Note that the interaction strength J has units of energy and a_c is a length scale that will equal the site spacing in the tight-binding case. The incoming kinetic energy of the DAE is given not by the tight-binding dispersion [Eq. (14)] but rather the continuum dispersion

$$K_{i,c} = \frac{\hbar^2 k_i^2}{2m_e} = t_c k_i^2 a_c^2 \quad \text{(B2)}$$

where k_i is its incoming wave number, m_e is its mass, and $t_c \equiv \hbar^2/2m_e a_c^2$ is an energy scale that will equal the hopping amplitude in the tight-binding case. Reference [19] finds that the transmission coefficient for the spin-flip scattering process $|\downarrow\rangle_e|\uparrow\rangle_1 \rightarrow |\uparrow\rangle_e|\downarrow\rangle_1$ is

$$T_{f,c} = \frac{J_0^2}{1 + \frac{5}{2}J_0^2 + \frac{9}{16}J_0^4} \quad \text{(B3)}$$

where the dimensionless parameter $J_0 \equiv \sqrt{2s}J/4t_c k_i a_c$. Likewise, the transmission coefficient for a no-spin-flip scattering process $|\downarrow\rangle_e|\uparrow\rangle_1 \rightarrow |\downarrow\rangle_e|\uparrow\rangle_1$ is

$$T_{\mathrm{nf,c}} = \frac{1 + \frac{1}{4}J_0^2}{1 + \frac{5}{2}J_0^2 + \frac{9}{16}J_0^4}. \quad \text{(B4)}$$

We now show that the tight-binding Green's-function solution we developed in Sec. II replicates the continuum solution, i.e., Eqs. (B3) and (B4). We then focus on two special cases that were not addressed by the continuum solution, but that our tight-binding solution can handle: inelastic scattering and an interaction with spatial degrees of freedom.

1. Replication of the continuum solution for a contact interaction

We now consider a tight-binding system with site spacing $a = a_c$ and hopping amplitude $t = t_c$. The first task for replicating the continuum solution is to approximate the continuum dispersion, Eq. (B2). For $k_i a \ll 1$, our tight-binding dispersion, Eq. (14), can be written

$$K_i = 2t - 2t\left[1 - \tfrac{1}{2}k_i^2 a^2 + O\left(k_i^4 a^4\right)\right]$$
$$= t k_i^2 a^2 + O\left(k_i^4 a^4\right). \quad \text{(B5)}$$

In other words, our tight-binding dispersion is a good approximation of the continuum dispersion in the case $k_i a \ll 1$. Our baseline expectation is that our results will be a good approximation for $k_i a \leqslant 0.1$ corresponding to $K_i/t \leqslant 0.01$.

The second task for replicating the continuum solution is to approximate the continuum scattering potential, Eq. (B1). This potential specifies a contact interaction in the sense that the DAE only interacts with the spin-1/2 particle when they are at the same point in space. We will approximate this scattering potential by specifying the $\boldsymbol{\varepsilon}_j$ operators $\boldsymbol{\varepsilon}_j$ [which determine the Hamiltonian according to Eq. (10)] as

$$\boldsymbol{\varepsilon}_j = \frac{J}{\hbar^2} \mathbf{S}_e \cdot \mathbf{S}_1 \delta_{j1}. \quad \text{(B6)}$$

When comparing Eq. (B6) to Eq. (B1), the question to consider is whether the discrete spatial interval a approximates the single continuous point $x = 0$. If the DAE's incoming wavelength $2\pi/k_i$ is much larger than the spatial interval a, than the DAE should not be sensitive to whether the space is discretized or not. This amounts to $k_i a \ll 2\pi$ which is included in the limit $k_i a \ll 1$ already adopted to replicate the continuum dispersion. We conclude that in the case $k_i a \ll 1$ our tight-binding transmission coefficients, calculated using Eq. (A11), should replicate Eqs. (B3) and (B4). To verify this using Eq. (B6), it is convenient to introduce the identity

$$\mathbf{S}_e \cdot \mathbf{S}_1 = S_e^z S_1^z + \tfrac{1}{2}(S_e^+ S_1^- + S_e^- S_1^+)$$

where the raising and lowering operators $S_l^\pm$ act on the eigenbasis of a spin-1/2 particle according to $S_l^+|\uparrow\rangle_l = 0$, $S_l^+|\downarrow\rangle_l = \hbar|\uparrow\rangle_l$, $S_l^-|\uparrow\rangle_l = \hbar|\downarrow\rangle_l$, and $S_l^-|\downarrow\rangle_l = 0$. As a result, we can write out the action of Eq. (B6) in the two-particle spin space:

$$\boldsymbol{\varepsilon}_j = \frac{J}{4}\delta_{j1} \begin{pmatrix} 1 & 0 & 0 & 0 \\ 0 & -1 & 2 & 0 \\ 0 & 2 & -1 & 0 \\ 0 & 0 & 0 & 1 \end{pmatrix} \begin{matrix} |\uparrow\rangle_e|\uparrow\rangle_1 \\ |\uparrow\rangle_e|\downarrow\rangle_1 \\ |\downarrow\rangle_e|\uparrow\rangle_1 \\ |\downarrow\rangle_e|\downarrow\rangle_1 \end{matrix}. \quad \text{(B7)}$$

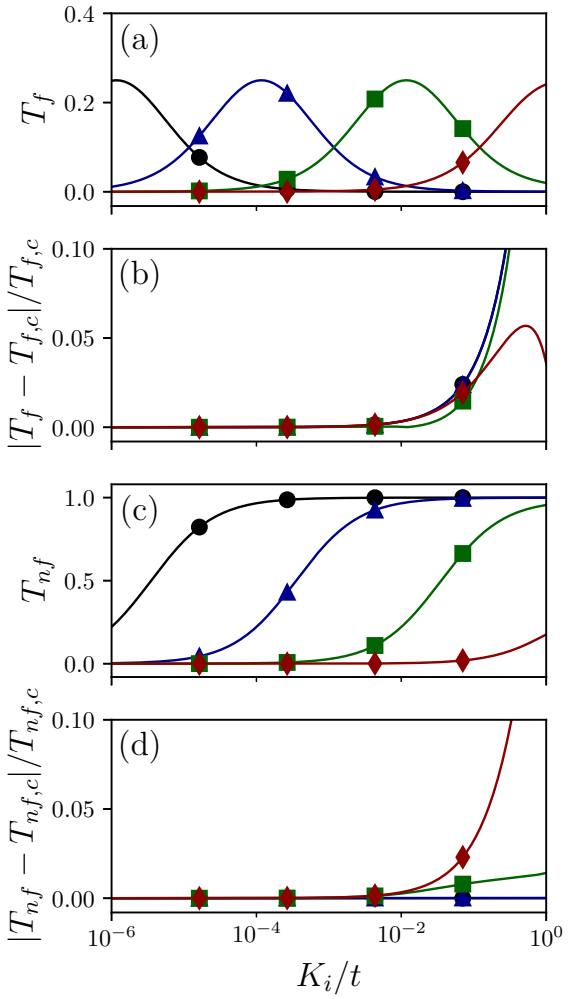

FIG. 9. (a) Spin-flip transmission probability from our tight-binding result and (b) its relative error. (b) No spin-flip transmission probability from our tight-binding result and (d) its relative error. Tight-binding parameters are $N = 1$ and $t = 1.0$ while the interaction strength J is given by (black circles) $J/t = -0.005$, (blue triangles) $J/t = -0.05$, (green squares) $J/t = -0.5$, and (red diamonds) $J/t = -5.0$.

Using Eq. (B7), our tight-binding solution yields transmission coefficients that replicate the continuum results when $K_i/t \ll 1$, as shown in Fig. 9. The relative error on our results is less than 0.01 below the $K_i/t = 0.01$ threshold, as seen in Figs. 9(b) and 9(d). Note that increasing the value of J impacts neither this threshold nor the amplitude of the T_f peaks. However, J does increase both the kinetic energy at which those peaks occur and the K_i/t value at which $T_{nf} \to 1$.

2. Inelastic scattering

Our system of interest involves spin degrees of freedom which may absorb energy during the scattering. As a result, the incoming and outgoing wave numbers [Eq. (15)] are spin dependent, so inelastic scattering is possible. In this simple example system, inelastic scattering can be accomplished by a Zeeman term on the spin-1/2 particle. This corresponds to

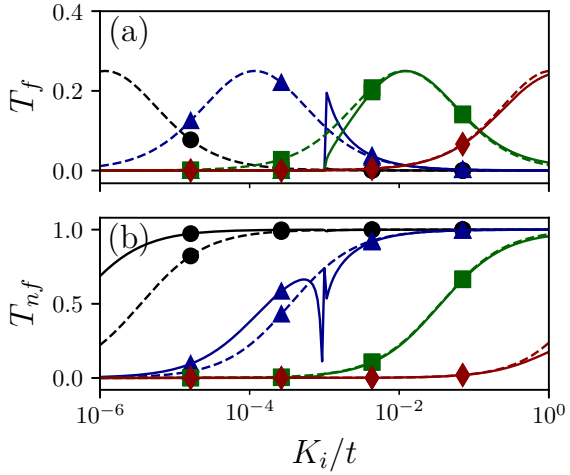

FIG. 10. (a) Spin-flip transmission probability from (solid) our tight-binding result and (dashed) the continuum result $T_{f,c}$. (b) No spin-flip transmission probability from (solid) our tight-binding result and (dashed) the continuum result $T_{nf,c}$. Tight-binding parameters are $N = 1$, $t = 1.0$, and $\Delta/t = 0.001$ while the interaction strength J is given by (black circles) $J/t = -0.005$, (blue triangles) $J/t = -0.05$, (green squares) $J/t = -0.5$, and (red diamonds) $J/t = -5.0$.

adding to Eq. (B7) the Zeeman operator

$$\frac{\Delta}{\hbar}\left(S_1^z + \frac{1}{2}\right) = \Delta \begin{pmatrix} 1 & 0 & 0 & 0 \\ 0 & 0 & 0 & 0 \\ 0 & 0 & 1 & 0 \\ 0 & 0 & 0 & 0 \end{pmatrix} \begin{matrix} |\uparrow\rangle_e|\uparrow\rangle_1 \\ |\uparrow\rangle_e|\downarrow\rangle_1 \\ |\downarrow\rangle_e|\uparrow\rangle_1 \\ |\downarrow\rangle_e|\downarrow\rangle_1 \end{matrix}. \tag{B8}$$

As shown in Fig. 10, the result is that T_f is forbidden when $K_i < \Delta$, suddenly turns on at $K_i = \Delta$, and returns to the $\Delta = 0$ continuum result when $\Delta \ll K_i \ll t$, before finally starting to diverge from the continuum result again when $K_i \to t$.

3. Physical origin of the Kondo-like interaction

Our solution specifies the reflection and transmission coefficients [Eqs. (A11) and (A13)] in terms of the retarded Green's function [Eq. (11)]. As formulated, the σ indices encode many-body spin degrees of freedom. However, these indices could be used to represent many-body quantum numbers besides spin, so our approach is generally applicable to interacting Hamiltonians. As an example, consider the Anderson model, which describes the Coulomb interaction between a conduction band electron and an electron in a localized orbital [29]. The Anderson model describes the physical origin of the Kondo-like interaction we have used throughout because a Schrieffer-Wolff transformation of this model allows the electrons to interact via their spins rather than their charges [29].

Consider a scattering region of size $N = 2$ containing two sites $j = 1, 2$ with hopping t_h between them. A single electron occupying site j has energy ε_j and two electrons occupying site j experience Coulomb repulsion U_j. For a system of two

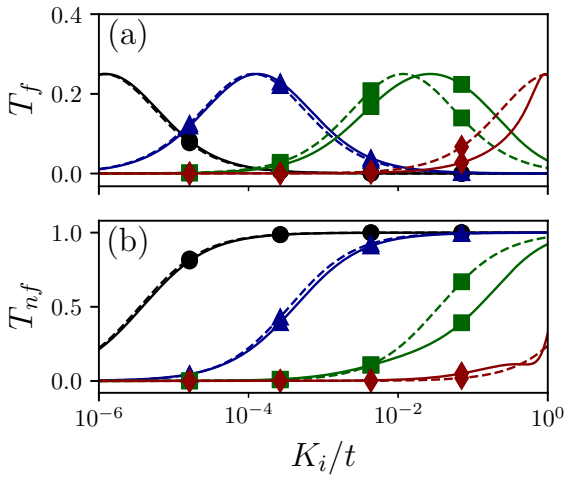

FIG. 11. (a) Spin-flip transmission probability from (solid) our tight-binding result and (dashed) the continuum result $T_{f,c}$. (b) No spin-flip transmission probability from (solid) our tight-binding result and (dashed) the continuum result $T_{nf,c}$. Tight-binding parameters are $N = 1$, $t = t_h = 1.0$, $U_1 = 0.0$, $U_2 = 100.0$. Using the prefactor of Eq. (B10) we set (black circles) $\varepsilon = 156.2$, $J/t = -0.005$; (blue triangles) $\varepsilon = 30.6$, $J/t = -0.05$; (green squares) $\varepsilon = 3.9$, $J/t = -0.5$; and (red diamonds) $\varepsilon = -0.4$, $J/t = -5.0$.

antiparallel electrons, the Anderson Hamiltonian is [30]

$$H_A = \varepsilon\hat{I} + \begin{pmatrix} U_1-\varepsilon & -t_h & t_h & 0 \\ -t_h & 0 & 0 & -t_h \\ t_h & 0 & 0 & t_h \\ 0 & -t_h & t_h & U_2+\varepsilon \end{pmatrix} \begin{matrix} |\uparrow\downarrow\rangle_1|\,\rangle_2 \\ |\uparrow\rangle_1|\downarrow\rangle_2 \\ |\downarrow\rangle_1|\uparrow\rangle_2 \\ |\,\rangle_1|\uparrow\downarrow\rangle_2 \end{matrix}, \quad \text{(B9)}$$

where $\varepsilon \equiv \varepsilon_2 - \varepsilon_1$. Care must be taken before inserting Eq. (B9) directly into the Hamiltonian [Eq. (10)] because the "spin" basis $|\sigma\rangle = \{|\uparrow\downarrow\rangle_1|\rangle_2, |\uparrow\rangle_1|\downarrow\rangle_2, |\downarrow\rangle_2|\uparrow\rangle_2, |\rangle_1|\uparrow\downarrow\rangle_2\}$ also contains spatial degrees of freedom in the doubly occupied states. We plainly cannot "transmit" the state $|\uparrow\downarrow\rangle_1|\rangle_2$.

The first way around this is to interpret the system as a one-dimensional chain of sites $j = \ldots, 0, 1, 3, \ldots$ where the site $j = 1$ is coupled to an off-chain site $j = 2$ which together form the scattering region. Both electrons can move freely in the scattering region, but only one electron can continue into the leads. Mathematically, this corresponds to modifying the hopping matrix $\mathbf{t} = t\mathbf{I}$ in Eq. (10) to $\mathbf{t} = \mathrm{diag}(0, t, t, 0)$.

Alternatively, we can ignore the double occupancy states, which are higher in energy, instead focusing on the lower-energy subspace $\{|\uparrow\rangle_1|\downarrow\rangle_2, |\downarrow\rangle_2|\uparrow\rangle_2\}$. Mathematically, this is accomplished by a Schrieffer-Wolff transformation [29], an expansion to second order in the small quantities $t_h/|U_1 - \varepsilon|$ and $t_h/|U_2 + \varepsilon|$ [30]. The resulting Schrieffer-Wolff Hamiltonian is [30]

$$\begin{aligned} H_{\mathrm{SW}} &= \left[\frac{-t_h^2(U_1+U_2)}{(U_1-\varepsilon)(U_2+\varepsilon)}\right]\begin{pmatrix} 1 & -1 \\ -1 & 1 \end{pmatrix}\begin{matrix} |\uparrow\rangle_1|\downarrow\rangle_2 \\ |\downarrow\rangle_1|\uparrow\rangle_2 \end{matrix} \\ &= \left[\frac{2t_h^2(U_1+U_2)}{(U_1-\varepsilon)(U_2+\varepsilon)}\right]\left(\frac{1}{\hbar^2}\mathbf{S}_1\cdot\mathbf{S}_2 - \frac{1}{4}\mathbf{I}\right). \end{aligned} \quad \text{(B10)}$$

This is the Kondo-like exchange interaction studied throughout this paper. The quantity in square brackets gives the interaction strength J. Note that, for $U_1 = U_2 = 0$, $J = 0$, revealing that the interaction is rooted in the Coulomb repulsion between the two electrons. Contrary to the geometrical interpretation of Eq. (B9), in Eq. (B10) the spatial degrees of freedom of the off-chain site $j = 2$ have been combined with the spin degrees of freedom of the on-chain site $j = 1$, i.e., the system has an effectively one-dimensional geometry.

Our solution allows us to implement either the exact Anderson Hamiltonian by setting $\boldsymbol{\varepsilon}_j = (H_A + \frac{J}{4}\mathbf{I})\delta_{1j}$ or the perturbative Schrieffer-Wolff Hamiltonian by setting $\boldsymbol{\varepsilon}_j = (H_{\mathrm{SW}} + \frac{J}{4}\mathbf{I})\delta_{1j}$, removing the constant energy shift in both cases to isolate the dot product of spin operators. We took the latter approach throughout this paper, and benchmarked it in Fig. 9. In Fig. 11 we benchmark the former approach at different values of J/t. We specify J/t by setting ε, and this determines the small quantities $t_h/|U_1 - \varepsilon|$ and $t_h/|U_2 + \varepsilon|$. One of these quantities always increases with increasing J, hurting the validity of the Schrieffer-Wolff transformation. Indeed, in Fig. 11 we see that the breakdown in the agreement at larger K_i/t is made worse when J/t is larger.

Although the solution to the spin-dependent scattering problem that we have just demonstrated incorporates first-principles descriptions of molecular magnetic systems and accounts for the spatial degrees of freedom of the delocalized electron, it is not a complete description. First, it would be interesting to incorporate the full orbital degrees of freedom in addition to the spin degrees of freedom. As demonstrated in this Appendix, our solution is capable of this task. Second, while we have considered only a single delocalized electron, a full treatment of the leads must recognize the presence of an entire conduction band, leading to Kondo effects. This is beyond the scope of our solution, requiring a many-body description.

[1] Michael Nielsen and Isaac Chuang, *Quantum Computation and Quantum Information: 10th Anniversary Edition* (Cambridge University, Cambridge, England, 2011).
[2] C. H. Bennett and D. P. DiVincenzo, Quantum information and computation, Nature (London) **404**, 247 (2000).
[3] G. Castagnoli and D. R. Finkelstein, Theory of the quantum speed-up, Proc. R. Soc. A **457**, 1799 (2001).
[4] M. Atzori and R. Sessoli, The second quantum revolution: Role and challenges of molecular chemistry, J. Am. Chem. Soc. **141**, 11339 (2019).
[5] M. Atzori, E. Morra, L. Tesi, A. Albino, M. Chiesa, L. Sorace, and R. Sessoli, Quantum coherence times enhancement in vanadium(IV)-based potential molecular qubits: The key role of the vanadyl moiety, J. Am. Chem. Soc. **138**, 11234 (2016).
[6] J. M. Zadrozny, J. Niklas, O. G. Poluektov, and D. E. Freedman, Millisecond coherence time in a tunable molecular electronic spin qubit, ACS Cent. Sci. **1**, 488 (2015).
[7] A. Gaita-Ariño, F. Luis, S. Hill, and E. Coronado, Molecular spins for quantum computation, Nat. Chem. **11**, 301 (2019).

[8] G. Burkard, D. Loss, and D. P. DiVincenzo, Coupled quantum dots as quantum gates, Phys. Rev. B **59**, 2070 (1999).

[9] D. Loss and D. P. DiVincenzo, Quantum computation with quantum dots, Phys. Rev. A **57**, 120 (1998).

[10] A. T. Costa, Jr., S. Bose, and Y. Omar, Entanglement of Two Impurities through Electron Scattering, Phys. Rev. Lett. **96**, 230501 (2006).

[11] E. D. Switzer, X.-G. Zhang, and T. S. Rahman, Anisotropy-exchange resonance as a mechanism for entangled state switching, Phys. Rev. A **104**, 052434 (2021).

[12] E. D. Switzer, X.-G. Zhang, and T. S. Rahman, Electronic control and switching of entangled spin state using anisotropy and exchange in the three-particle paradigm, J. Phys. Commun. **6**, 075007 (2022).

[13] G. L. Giorgi and F. de Pasquale, Two-spin entanglement induced by electron scattering in nanostructures, Phys. Rev. B **74**, 153308 (2006).

[14] F. Ciccarello, M. Palma, M. Zarcone, Y. Omar, and V. R. Vieira, Entanglement controlled single-electron transmittivity, New J. Phys. **8**, 214 (2006).

[15] F. Ciccarello, G. M. Palma, M. Paternostro, M. Zarcone, and Y. Omar, Entanglement generation between two spin-s magnetic impurities in a solid via electron scattering, Solid State Sci. **11**, 931 (2009).

[16] K. Yuasa and H. Nakazato, Resonant scattering can enhance the degree of entanglement, J. Phys. A: Math. Theor. **40**, 297 (2007).

[17] G. Cordourier-Maruri, F. Ciccarello, Y. Omar, M. Zarcone, R. de Coss, and S. Bose, Implementing quantum gates through scattering between a static and a flying qubit, Phys. Rev. A **82**, 052313 (2010).

[18] F. Ciccarello, D. E. Browne, L. C. Kwek, H. Schomerus, M. Zarcone, and S. Bose, Quasideterministic realization of a universal quantum gate in a single scattering process, Phys. Rev. A **85**, 050305(R) (2012).

[19] O. L. T. de Menezes and J. S. Helman, Spin flip enhancement at resonant transmission, Am. J. Phys. **53**, 1100 (1985).

[20] P. A. Khomyakov, G. Brocks, V. Karpan, M. Zwierzycki, and P. J. Kelly, Conductance calculations for quantum wires and interfaces: Mode matching and Green's functions, Phys. Rev. B **72**, 035450 (2005).

[21] S. J. Tans, M. H. Devoret, H. Dai, A. Thess, R. E. Smalley, L. J. Geerligs and C. Dekker, Individual single-wall carbon nanotubes as quantum wires, Nature (London) **386**, 474 (1997).

[22] M.-V. Fernandez-Serra, Ch. Adessi, and X. Blase, Conductance, surface traps, and passivation in doped silicon nanowires, Nano Lett. **6**, 2674 (2006).

[23] M. Urdampilleta, S. Klyatskaya, J.-P. Cleuziou, M. Ruben, and W. Wernsdorfer, Supramolecular spin valves, Nat. Mater. **10**, 502 (2011).

[24] H. Aurich, A. Baumgartner, F. Freitag, A. Eichler, J. Trbovic, and C. Schönenberger, Permalloy-based carbon nanotube spin-valve, Appl. Phys. Lett. **97**, 153116 (2010).

[25] D. Kalkstein and P. Soven, A Green's function theory of surface states, Surf. Sci. **26**, 85 (1971).

[26] J. Velev and W. Butler, On the equivalence of different techniques for evaluating the Green function for a semi-infinite system using a localized basis, J. Phys.: Condens. Matter **16**, R637 (2004).

[27] R. Haydock, V. Heine, and M. Kelly, Electronic structure based on the local atomic environment for tight-binding bands, J. Phys. C: Solid State Phys. **5**, 2845 (1972).

[28] A. MacKinnon, The calculation of transport properties and density of states of disordered solids, Z. Phys. B **59**, 385 (1985).

[29] J. R. Schrieffer and P. A. Wolff, Relation between the Anderson and Kondo Hamiltonians, Phys. Rev. **149**, 491 (1966).

[30] E. Koch, *The Physics of Correlated Insulators, Metals, and Superconductors* (Verlag des Forschungszentrum Jülich, Jülich, 2017), Chap. 4.

[31] R. Vincent, S. Klyatskaya, M. Ruben, W. Wernsdorfer, and F. Balestro, Electronic read-out of a single nuclear spin using a molecular spin transistor, Nature (London) **488**, 357 (2012).

[32] R. Shankar, *Principles of Quantum Mechanics*, 2nd ed. (Plenum, New York, 1994).

[33] F. Verstraete, M. Popp, and J. I. Cirac, Entanglement versus Correlations in Spin Systems, Phys. Rev. Lett. **92**, 027901 (2004).

[34] J.-X. Yu, G. Christou, and H.-P. Cheng, Analysis of exchange interactions in dimers of Mn_3 single-molecule magnets, and their sensitivity to external pressure, J. Phys. Chem. C **124**, 14768 (2020).

[35] H. Park, S. Liu, J. N. Fry, and H.-P. Cheng, First-principles study of bilayer polymeric manganese phthalocyanine, Phys. Rev. B **105**, 195408 (2022).

[36] G. Rajaraman, E. C. Sañudo, M. Helliwell, S. Piligkos, W. Wernsdorfer, G. Christou, and E. K. Brechin, Magnetic and theoretical characterization of a ferromagnetic Mn(III) dimer, Polyhedron **24**, 2450 (2005).

[37] W. Wernsdorfer, N. Aliaga-Alcalde, D. N. Hendrickson, and G. Christou, Exchange-biased quantum tunnelling in a supramolecular dimer of single-molecule magnets, Nature (London) **416**, 406 (2002).

[38] S. Liu, M. Yazback, J. N. Fry, X.-G. Zhang, and H.-P. Cheng, Single-molecule magnet Mn_{12} on GaAs-supported graphene: Gate field effects from first principles, Phys. Rev. B **105**, 035401 (2022).

[39] Z. Hooshmand, J.-X. Yu, H.-P. Cheng, and M. R. Pederson, Electronic control of strong magnetic anisotropy in Co-based single-molecule magnets, Phys. Rev. B **104**, 134411 (2021).

[40] A. H. Follmer, R. D. Ribson, P. H. Oyala, G. Y. Chen, and R. G. Hadt, Understanding covalent versus spin-orbit coupling contributions to temperature-dependent electron spin relaxation in cupric and vanadyl phthalocyanines, J. Phys. Chem. A **124**, 9252 (2020).

[41] S. L. Bayliss, D. W. Laorenza, P. J. Mintun, B. Diler, D. E. Freedman, and D. D. Awschalom, Optically addressable molecular spins for quantum information processing, Science **370**, 1309 (2020).

[42] M. Zwierzycki, P. Khomyakov, A. A. Starikov, K. Xia, M. Talanana, P. X. Xu, V. Karpan, I. Marushchenko, I. Turek, E. W. Bauer, G. Brocks, and P. J. Kelly, Calculating scattering matrices by wave function matching, Phys. Status Solidi B **245**, 623(2008).